Chemical Engineering Journal 497 (2024) 154772

Contents lists available at ScienceDirect

Chemical Engineering Journal

journal homepage: www.elsevier.com/locate/cej

Superhydrophobic asymmetric pH-responsive soft actuators: Implications for the development of anti-fouling medical devices

Amit Kumar [a,c], Smruti Parimita [b], Kumari Kiran [a], Nitish R. Mahapatra [a], Pijush Ghosh [c,d,*]

[a] Department of Biotechnology, Bhupat and Jyoti Mehta School of Biosciences, Indian Institute of Technology Madras, Chennai 600036, India
[b] Manufacturing Engineering Section, Department of Mechanical Engineering, Indian Institute of Technology Madras, Chennai 600036, India
[c] Department of Applied Mechanics and Biomedical Engineering, Indian Institute of Technology Madras, Chennai 600036, India
[d] Center for Soft and Biological Matter, Indian Institute of Technology Madras, Chennai 600036, India

ARTICLE INFO

Keywords:
Superhydrophobic surface
Janus structure
pH-responsive
Soft actuators
Antifouling property
4D printing

ABSTRACT

Biomedical engineering strives for innovation to enhance the safety and effectiveness of medical tools, such as catheters and stents that need to be operated in confined spaces, with precise drug delivery control and should possess anti-fouling properties. Soft actuators with superhydrophobic surfaces can provide adaptable shape change together with non-fouling attributes required for medical devices. In this study, we have developed a Janus film with a hydrophilic solvent-responsive bottom and superhydrophobic top surface using a self-assembly strategy. The devised new strategy involves the dispersal of modified silica nanoparticles into a homogeneous solution, where they were segregated from the polymer matrix and self-assembled to form a superhydrophobic layer on the surface with a water contact angle of >150°. The resulting asymmetric actuator demonstrated bidirectional actuation in solvents with extreme pH values i.e., pH 1 and 13. It could be tailored for specific hydrophilicity by adjusting the ratio of dispersed superhydrophobic and hydrophilic silica nanoparticles in the polymer solution. These films exhibited exceptional chemical stability against strong acids, alkaline solutions, ethanol, and salt, as well as mechanical stability against abrasion from sandpaper. In vitro studies confirmed their superior anti-fouling and anti-bacterial properties. Furthermore, actuation of printed 3D structures with different patterns was demonstrated, showcasing the possibility of developing these superhydrophobic asymmetric surfaces via 3D printing and their potential as cardiovascular stents.

1. Introduction

Medical devices for surgery, endoscopy, and drug delivery require an acute or semi-chronic safe interaction with the human body. The device should not only provide smooth and effective contact and coupling with human parts but also need to mimic human tissues in terms of mechanical properties, motion, and function. Current conventional biomedical devices have limitations in frequent bacterial infection of urinary catheters leading to chronic infection [1], poor deliverability, platelet deposition of bioresorbable cardiovascular stent [2], damaging tissues, muscles, and blood vessels around a surgical site during minimally invasive surgery [3] and controlled drug delivery [4].

In the past 10 years, biomedical soft robots have been developed with key features such as controllable response to external stimuli, tunable mechanical properties, morphological adaptability to the biological environment, and functionally active. For applications such as catheters [5,6] and minimally invasive surgery [7,8], the soft actuator designed should not only mimic the structure of the desired tissue/part/component but also be able to perform functions such as drug delivery, cell growth, antibacterial, anticoagulant surface, etc., when placed at the targeted site. Therefore, a 3D-printed stimuli-responsive structure with a superhydrophobic surface can address the major requirement for the above-mentioned applications.

Stimuli-responsive polymers can undergo reversible/irreversible changes in their physicochemical properties in response to external stimuli such as temperature [9,10], light [11–14], electric fields [15,16], or chemical species like solvent [17–20] and pH [21–23]. A human body consists of body fluids that exist in different forms and have different concentrations of electrolytes and metabolites with different physiological pH. This provides a considerable advantage to solvent-responsive systems for various biomedical applications. Solvent-responsive polymers represent a class of materials that actuate in response to solvent

* Corresponding author at: Department of Applied Mechanics and Biomedical Engineering, Indian Institute of Technology Madras, Chennai 600036, India.
E-mail address: pijush@iitm.ac.in (P. Ghosh).

https://doi.org/10.1016/j.cej.2024.154772
Received 7 May 2024; Received in revised form 5 August 2024; Accepted 10 August 2024
Available online 11 August 2024
1385-8947/Published by Elsevier B.V.

medium. The nature of solvent-responsive actuation mainly depends on matrix property [19], solvent composition [22] and matrix solvent interaction. Chitosan is one such biocompatible smart polymer that responds to solvents. Chitosan thin films are prepared by solvent casting in plastic petridish and drying at room temperature for 20 h. When the chitosan thin film is placed on the solvent surface, the solvent molecules diffuse into the polymer matrix and create a concentration gradient across the thickness. The concentration gradient developed across the thickness results in a displacement field that leads to out-of-plane bending of the films. However, the chitosan film does not actuate when dipped inside the solvent as diffusion occurs from both sides, which does not allow the formation of the concentration gradient necessary for actuation. The control of solvent diffusion can be achieved by developing asymmetric films. Over the years, researchers have used different approaches to develop asymmetric films, i.e., a) by developing a crosslinking gradient across the thickness [19], b) by forming a porous gradient across the thickness [24], c) by forming a bilayer with either another hydrogel with different diffusion characteristics [22] or with hydrophobic polymer [25]. Attaining an asymmetric film with a superhydrophobic surface can bring desirable functional advantages such as antifouling and antiplatelet adhesion required for biomedical applications.

Superhydrophobicity is a property of many naturally occurring substrates, including lotus leaves [26,27], shark skin [28,29], rose petals [30], water strider legs [31,32], and butterfly wings [33,34]. Superhydrophobic surfaces have extremely high-water repellency and provide self-cleaning surfaces. Superhydrophobic surfaces have garnered significant interest due to their ability to offer non-fouling properties for biomedical applications such as cell scaffolds, medical devices, and bacterial inhibition. From the perspective of hydrophobic principles, the methods for developing superhydrophobic surfaces are divided into two types: a) by changing the roughness [35–37] and b) by reducing the surface energy via chemical modifications [38,39]. Inducing rough microstructure does have the advantage of reproducibility in large areas; however, at the same time, it is costly and susceptible to microstructure damage. Chemical modification via spray coating is a cost-effective method to develop a superhydrophobic surface, although it does exhibit poor adhesion strength.

This work presents a simple and efficient method to integrate superhydrophobic surfaces into a solvent-responsive soft actuator via self-assembly of Methyl Trichloro Silane (MTS)-modified silica nanoparticles (SiNPs). During drying, the nature of superhydrophobic particles to separate from hydrophilic solution led to the formation of a SiNP layer on the surface, a phenomenon observed by Iline-Vul et al. [40]. The asymmetric nature of the film not only provides responsiveness inside the solvent but also provides a superhydrophobic surface for biomedical applications. The actuation of the asymmetric film was controlled by varying the hydrophobicity. The developed asymmetric films showed bidirectional pH-responsive behavior, i.e., clockwise actuation in acidic pH (viz. 0.1 M HCl) and anti-clockwise direction in alkaline pH (viz. 0.1 M NaOH). The developed films exhibited exceptional chemical stability against strong acids, alkaline solutions, ethanol, and salt solutions, as well as mechanical stability against abrasion. In-vitro antibacterial adhesion, antibacterial activity, and bacterial infiltration studies were conducted to confirm the antifouling activity required for biomedical implants, most commonly cardiovascular implants (stents, heart valve replacements, central venous lines, etc.). A similar approach was followed for printing 3D asymmetric structures, which were shown to actuate into various architectures to further project their potential usage in biomedical applications.

2. Materials and methods

2.1. Materials

Chitosan powder (degree of deacetylation >90 %; viscosity, 100–200 cps; medium molecular weight), Toluene (99 %), (3-Aminopropyl)triethoxysilane (APTES) and Methyl trichlorosilane (MTS) were purchased from Avra chemicals, Hyderabad, India, Fumed Silica nanoparticles (NPs) were purchased from Astra chemicals, Chennai. Hydrochloric acid (37 %, ACS reagent), glutaraldehyde (25 % aqueous solution), and acetic acid (>99.7 %) were purchased from Sigma-Aldrich (India, Bangalore). For analysis, sodium hydroxide pellets (low chloride) were purchased from Merck Life Sciences, India. A petri dish of 9 cm diameter was used to pour a chitosan solution to make a film.

2.2. Preparation and characteristics of asymmetric MTS-modified SiNPs/chitosan

2.2.1. Preparation of MTS modified silica nanoparticles

First, 2 g of fumed silica (1 %) nanoparticles were mixed in 200 ml of toluene for 2 h. To the solution, 2 ml of methyl trichlorosilane (MTS) was added drop by drop with continuous stirring and kept for 2 h to ensure proper superhydrophobic modification of silica nanoparticles. The solution was poured into a glass Petri dish and left to dry in the oven overnight. The dried nanoparticles obtained are superhydrophobic, as shown in Fig. 1a.

2.2.2. Preparation of asymmetric MTS-modified SiNPs/chitosan

After the preparation of MTS-modified SiNPs (Superhydrophobic), homogenous solutions of CS (1.5 % (w/v)) were prepared by mixing 1.5 g of chitosan powder in a beaker containing 100 ml of 1 % (v/v) acetic acid solution. The mixture was stirred on a hot plate magnetic stirrer at 55 °C for 5 h.

The superhydrophobic silica nanoparticles were added to the prepared 1.5 % (w/v) chitosan solution in 1:1 and 2:1 (chitosan: silica NPs) by weight. The solution was stirred till the solution became cream-whitish. The solution was dried in a Petri dish at room temperature for 24 h.

During drying, the superhydrophobic SiNPs separate to the top and self-assemble themselves to form a layer on the surface. After complete drying, the films formed were asymmetric with a superhydrophobic surface and hydrophilic chitosan at the bottom, as presented in Fig. 1b.

The asymmetric films were prepared with varied layer thickness and hydrophobicity as shown in Fig. 2.

2.3. Characterisation of the asymmetric hydrophobic chitosan films

2.3.1. Fourier transform infrared spectroscopy (FTIR)

The Fourier transform infrared spectroscopy (FTIR) was done using a TENSOR II FTIR Spectrophotometer from Bruker Optics for chemical structure elucidation before and after superhydrophobic modification of silica NPs. The FTIR spectra were achieved from the top and bottom sides of the prepared films with a frequency range from 4000 to 400 cm^{-1}.

2.3.2. Scanning electron microscope (SEM)

The morphological features of the asymmetric MTS-modified chitosan films were characterized using a high-resolution scanning electron microscope (HR SEM) (ZEISS EVO-18) under an accelerating voltage of 1–3 kV. Dried films were frozen under liquid nitrogen and cut into small sections to maintain their interface structure. Samples were stuck on the SEM substrate using carbon tape, and then they were sputter-coated with a thin film for 120 sec using an ion coater (Hitachi E-1300) before SEM observation. The obtained images were used to analyze the thickness and interface of prepared films.

2.3.3. Transmission electron microscopy (TEM)

The size, morphology and surface properties of the MTS-modified silica nanoparticles were characterized using Transmission electron microscopy (TEM) (JOEL F200). The unmodified and modified particle dispersion was prepared in toluene with 1 h of ultrasonication. A drop

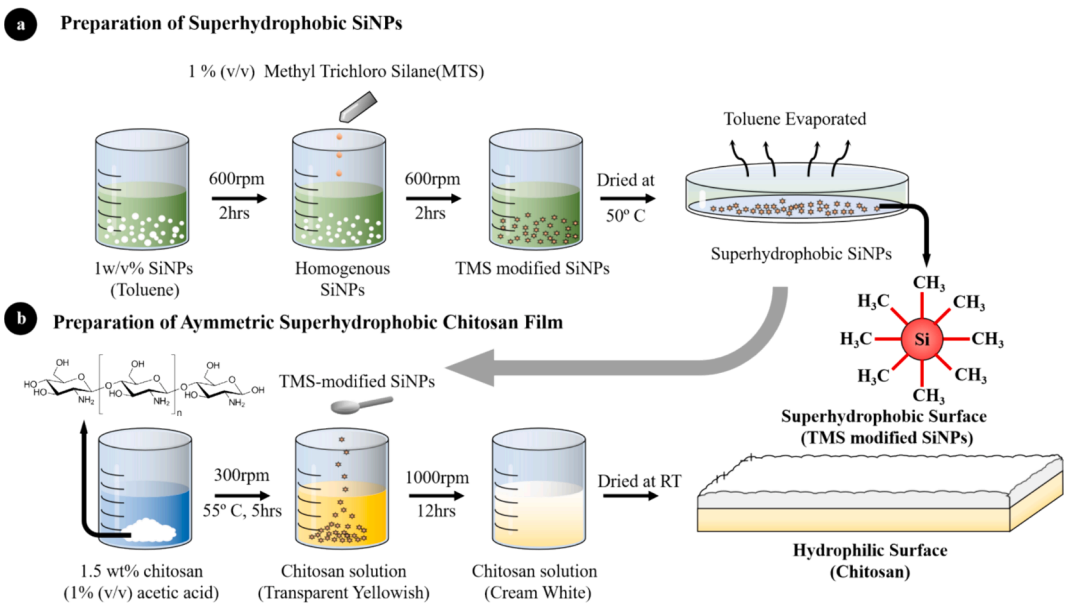

Fig. 1. Schematic illustration representing (a) the preparation of superhydrophobic silica nanoparticles with MTS to obtain –CH_3 on the SiNPs, (b) procedure for preparation of asymmetric chitosan films with MTS-modified SiNPs.

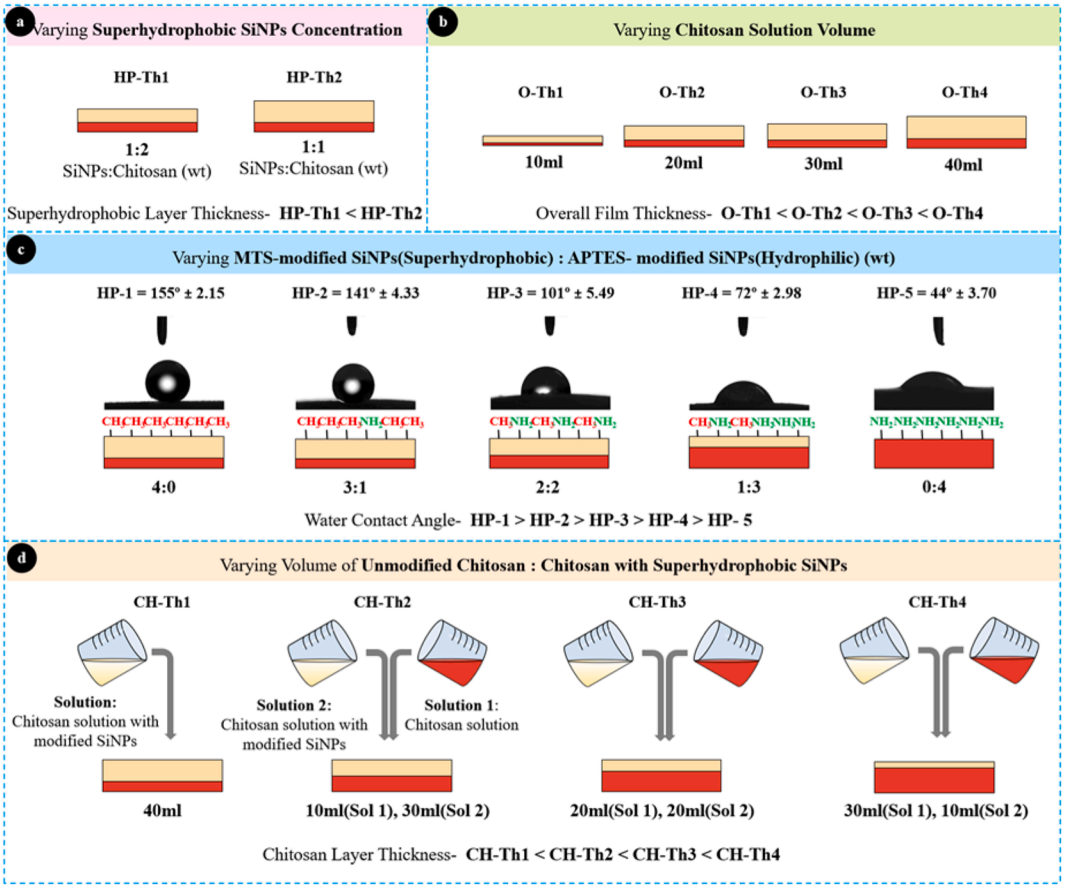

Fig. 2. Preparation of asymmetric chitosan films with (a) Fixed volume of 10 ml, different concentrations of superhydrophobic SiNPs in chitosan, (b) Fixed concentration of 1:1 (chitosan: SiNPs(wt)), different volumes of chitosan solution with superhydrophobic SiNPs, (c) varied concentration of MTS modified SiNPs and APTES modified SiNPs in chitosan solution for effect of film surface hydrophilicity on actuation, and (d) different volume ratio of chitosan solution with and without superhydrophobic SiNPs for pH-responsive actuation.

(~20 μl) was poured on a carbon tape-coated carbon grid to adhere the unmodified and modified SiNPs and was allowed to dry at room temperature overnight. The images and plot obtained were used to analyse the particle size, crystallinity and chemical composition.

2.3.4. Asymmetric wettability measurements (Water contact angle)

The wettability of the superhydrophobic surface was measured via sessile drop contact angle measurements with GBX digidrop contact angle meter. Water contact angle (WCA) on three samples: a water droplet of 8 μl was dispensed onto the hydrophobic surface of chitosan film, and the contact angle was measured. Each experiment was repeated 5 times at different points on the same sample.

2.3.5. Chemical stability

The chemical stability of superhydrophobic coatings was evaluated by immersing the prepared MTS-modified SiNPs/chitosan films (CH-Th4) (1 cm × 1 cm) in acidic solution (0.1 M HCl, pH = 1), alkaline solution (0.1 M NaOH, pH = 13), salt solution (1 M NaCl, pH = 7) and ethanol (100 % v/v) for 24 h, respectively, after which the water contact angle (WCA) was tested. Moreover, we evaluated the chemical stability of superhydrophobic coatings by exposing the sample to UV irradiation for 30 min. The UV irradiation source was provided by Quartz UVC germicidal lamps (wavelength = 253.7 nm), and the UV source was fixed at a height of 10 cm vertically from the sample. Each experiment was repeated 5 times at different points on the same sample.

2.3.6. Mechanical stability

The mechanical properties were measured by the sandpaper abrasion test using 400 grit SIC sandpaper on CH-Th4 films. The hydrophobic outer layer of chitosan film (1 cm × 1 cm) was placed face-down to the sandpaper, and a 100 g weight was placed on top of the samples. The sample was moved 10 cm to and fro along the direction parallel to the edge of the sandpaper. One movement of 10 cm to and fro is one abrasion cycle. The water contact angle (WCA) was measured after each abrasion cycle.

2.3.7. Swelling ratio

The swelling behavior of different concentrations and thicknesses of the films was studied using gravimetric measurements. Specimens cut into specified dimensions (1 cm × 1 cm square) were weighed and immersed in deionised water, 0.1 M HCl, and 0.1 M NaOH at room temperature. The swollen samples were weighed at different time intervals till the samples reached a constant weight, indicating equilibrium swelling.

The swelling ratio (SR) was calculated as $SR = \frac{W_s - W_d}{W_s} \times 100\%$, where W_s and W_d respectively denote the films' swollen weight and dry weight, and an average of five measurements after 4 h was reported.

2.4. Actuation characterisation

Prepared asymmetric films were cut into 10 mm × 2 mm rectangular strips. Actuation videos were recorded in DI water, acid solution (pH 1 & pH 4), and basic solution (pH 10 & pH 13) and analyzed using ImageJ software. Then, using analyzed images, an X-Y displacement plot was obtained using MATLAB software.

2.5. Antibacterial activity

2.5.1. Bacterial adhesion assay

The bacterial adhesion assay was performed by putting 50 μl of *E. coli* DH5α(gram-negative) and *S. aureus* RN4220(gram-positive) strains suspension (1×10^8) on the superhydrophobic side of chitosan films of 1 cm × 1 cm dimension. The samples were incubated for 1 h at 37 °C. Then, the samples were washed with PBS three times to remove nonattached bacteria and immersed into 4 % glutaraldehyde in PBS overnight at 4 °C. The samples were then dehydrated in 70 % (v/v) ethanol. Finally, bacterial adhesion was visualized by SEM.

2.5.2. Antibacterial activity test

The antibacterial activities of the superhydrophobic surface against *E. coli* DH5α(gram-negative) and *S. aureus* RN4220(gram-positive) were determined using the streak plate method. The samples were UV sterilized and were dipped in ethanol to avoid any contamination. 50 μl of *E. coli* and *S. aureus* suspension (1×10^8 CFU/ml) were kept on the superhydrophobic side of asymmetric chitosan films of 1 cm × 1 cm dimension. The samples were incubated for 2 h at 37 °C. Then, the samples were washed to remove unattached bacteria. The samples were kept in an incubator.

After incubation, viable bacteria were quantified by streak plate methods, where the films with bacterial cells were streaked on an LB agar plate. The plates were kept in an incubator and visualized after 24 h.

2.5.3. Bacteria infiltration test

First, the samples were placed under UV light for irradiation sterilization and dipped in ethanol (70 % v/v). The sterile square (1 cm × 1 cm) pieces of the films were placed on LB plates with the superhydrophobic surface up. Then, 50 μl of bacterial suspension (~10^8 CFU/ml) was dropped on each hydrophobic surface and incubated at 37 °C for 24 h. The films were removed, and the growth of bacteria in the plate was observed and visualized after 24 h.

2.5.4. Quantitative antibacterial tests

The quantitative anti-bacterial test was performed with pristine chitosan film as a control and asymmetric film as a sample. First, the samples were placed under UV light for irradiation sterilisation and dipped in ethanol (70 % v/v). 50 μl of *E. coli* and *S. aureus* suspension (1×10^8 CFU/ml) were kept on the superhydrophobic side of asymmetric chitosan films of 1 cm × 1 cm dimension. The samples were incubated for 2 h at 37 °C. Then, the samples were washed with PBS one time to remove non-attached bacteria, and the second was with PBS collected. 100 μl of collected samples were added to 1 ml nutrient media (dilution = 10-fold). Serial dilution was done till 10^4 dilutions. The bactericidal efficacy of samples was characterized using the spread plate method, where 100 μl of bacterial suspensions were extracted using micropipettes and inoculated onto agar plates. The number of CFU was visually inspected after incubating at 37 °C for 24 h. After 18 h of incubation of collected samples, the Abs600 measurements were done. The absorbance of nutrient broth (1 ml) without bacteria was used as the blank reference.

2.6. Data presentation and statistical analysis

All the actuation experiments were repeated 15 times. Using GraphPad Prism software, statistical analysis was carried out by one-way and two-way analysis of variance (ANOVA) with Tukey's and Sidak's multiple comparison post-test. The curvature plots are representative of the X–Y displacement profile of one sample from 10 samples.

3. Results and discussion

3.1. Actuation mechanism

The mechanism for the actuation of SiNP-modified chitosan films can be understood by first understanding the actuation of unmodified chitosan films. Chitosan films have shown solvent-responsive behavior as described in [11,12]. Briefly, as a chitosan film is kept on the solvent (one side exposed to solvent), the solvent molecules diffuse into the chitosan matrix and migrate towards the other end. The diffusion of solvent from one end (in contact with solvent) to the other end leads to

the development of a concentration gradient across the thickness of the film, giving rise to displacement or strain gradient, resulting in out-of-plane folding of the film. As the solvent continues to diffuse inside the polymer matrix, the concentration gradient diminishes, causing the film to unfold. However, when dipped inside the solvent, the pristine film does not actuate since solvent diffusion occurred from both sides, resulting in no gradient formation. As shown in Fig. 3a, the snapshots show no actuation after 40 sec of being dipped inside the solvent.

The asymmetric film was prepared with 40 ml chitosan solution with a 1:2 (SiNPs: chitosan) mixing ratio and dried at room temperature for 24 h. The asymmetric chitosan films prepared by MTS-modified SiNPs contain a superhydrophobic layer on one side and hydrophilic chitosan on the other. When the prepared asymmetric films were dipped inside the solvent, the film actuated due to solvent diffusion from the hydrophilic surface. In contrast, the superhydrophobic layer does not allow any diffusion, as shown in Fig. 3b. As demonstrated in Fig. 3b, the asymmetric film took 20 sec to fold completely. The diffusion of a solvent through one side leads to a concentration gradient across the thickness of the film, thus giving rise to actuation under the solvent. Because of the presence of superhydrophobic layer on top, the concentration gradient is always maintained inside the polymer, as illustrated, causing a permanent or irreversible folding of the matrix.

3.2. Actuation of asymmetric MTS-modified SiNPs/chitosan film

Asymmetric superhydrophobic films were prepared by mixing MTS-modified silica nanoparticles (superhydrophobic) (Fig. S9) in chitosan solution in varied quantities. A clear, distinguished, self-assembled superhydrophobic SiNP separates to the top surface during drying, as shown in Fig. S1. The mechanical characterization of the developed asymmetric can be found in Fig. S7. The actuation of prepared asymmetric film depends on a) superhydrophobic SiNPs (top surface) layer thickness, b) chitosan (bottom layer) thickness, c) complete bilayer thickness, and d) hydrophilicity of top surface as shown in Fig. 2.

In this section, the actuation characteristics were obtained for asymmetric films prepared by a) attaining different superhydrophobic layer thicknesses and b) overall bilayer thickness. The overall thickness of the film and SiNPs layer on the top surface after drying depends on the volume of the prepared solution and the concentration of SiNPs in the chitosan solution, respectively.

The actuation behavior of prepared asymmetric films was demonstrated by dipping the film underwater. The films were cut into 10 mm $\times$ 2 mm rectangular strips, and actuation was recorded for the cantilever films. The superhydrophobic layer thickness of HP-Th1(1:2) and HP-Th2 (1:1) was found to be 97.14 μm (total film thickness- 124.3 μm) and 33.53 μm (total film thickness- 68.19 μm) respectively, obtained by film prepared by changing the concentration of superhydrophobic SiNPs (by weight) in 10 ml chitosan solution, as shown in Fig. 4a1 and Fig. 4a2. The actuation of prepared asymmetric film was plotted in Fig. 4b. The plot shows the actuation time when the films prepared with different concentrations of SiNPs were placed in DI water, the HP-Th2 film actuated completely in 3.3 $\pm$ 0.5 sec, whereas the HP-Th1 film actuated in 0.6 $\pm$ 0.22 sec (two-way ANOVA followed by Sidak's multiple comparison test, P = 0.0017; Fig. 4b). More thickness of the HP-Th2 film makes it stiffer compared to HP-Th1 film thus resulted in slower actuation.

By increasing the volume of the prepared solution with the same ratio of superhydrophobic SiNPs, the films O-Th1, O-Th2, O-Th3, and O-Th4 with increased overall thickness were attained, as shown in Fig. S2. The films O-Th1, O-Th2, O-Th3, and O-Th4 actuated completely in 3.33 $\pm$ 0.5 sec, 7.67 $\pm$ 1.15 sec, 27 $\pm$ 2.64 sec, and 35.3 $\pm$ 0.58 sec, respectively, for 1:1 SiNPs to chitosan ratio (by wt). Similarly, the films O-Th1, O-Th2, O-Th3, and O-Th4 actuated completely in 0.6 $\pm$ 0.22 sec, 3.67 $\pm$ 1.15 sec, 11 $\pm$ 3.05 sec, and 24 $\pm$ 1 sec, respectively, for 1:2 SiNPs to chitosan ratio (by wt) as plotted in Fig. 4b. The difference in actuation time of O-Th1, O-Th2, O-Th3 and O-Th4 were statistically significant (two-way ANOVA followed by Tukey's multiple comparison test, P < 0.0001). The films with more overall thickness actuated at a slower rate due to the increased stiffness of the film. Fig. 4c shows the curvature acquired by the films while actuating at an instant of time.

3.3. Effect of tuned surface hydrophobicity on actuation of asymmetric films

In the above section, the role of superhydrophobic layer thickness on the actuation was studied by varying the volume and modified SiNPs. Desirable actuation characteristics can also be tuned and attained by changing the surface hydrophobicity. To vary the hydrophobicity of the matrix, APTES-modified SiNPs (hydrophilic) along with MTS-modified SiNPs (Superhydrophobic). Unmodified SiNPs are hydrophilic because of –OH groups; our hypothesis was to attain super hydrophilic SiNPs using APTES modification by incorporating $–NH_2$ groups. The water contact angle obtained was reduced to 44° $\pm$ 3 for APTES-modified SiNPs, however, they were not super hydrophilic as hypothesized. In this section, the hydrophobicity was varied using different ratios of MTS-modified SiNPs (superhydrophobic) and APTES-modified SiNPs (hydrophilic). In Fig. 5a, a superhydrophobic surface (HP-1) is illustrated with methyl groups ($–CH_3$) from MTS-modified SiNPs exposed on the surface, and a hydrophilic surface (HP-5) is described with amine groups ($–NH_2$) from APTES-modified SiNPs exposed.

The change in hydrophilicity of the prepared films HP-1, HP-2, HP-3, HP-4, and HP-5 was obtained with different ratios of the MTS-modified SiNPs to APTES-modified SiNPs, i.e., 4:0, 3:1, 2:2, 1:3 and 0:4 (by weight) respectively. The contact angle of prepared samples was found to be 155° $\pm$ 2.15 (HP-1), 141° $\pm$ 4.33 (HP-2), 101° $\pm$ 5.49 (HP-3), 72° $\pm$ 2.98 (HP-4), 44° $\pm$ 3.70 (HP-5) as shown in Fig. 2c, and 87° $\pm$ 4.68 (pristine chitosan). As shown in Fig. 5b, the observed contact angle reduced from 155° $\pm$ 2.15 to 44° $\pm$ 3.70 with a reduction in MTS-modified SiNPs concentration and were statistically different (one-way ANOVA, F=640.7, P < 0.0001). Varying hydrophilicity forms asymmetric films with contact angle differences between the top and bottom surfaces. The contact angle is directly linked to the interaction of the solvent with the matrix, thereby affecting the diffusion characteristic of the solvent (water). The difference in solvent diffusion from the top and bottom surface leads to differential swelling across the thickness, affecting the total folding time, rate, and extent of actuation.

The HP-1 and HP-2 films with a high ratio of superhydrophobic SiNPs, actuated completely in 8 $\pm$ 1 sec and 20 $\pm$ 3 sec, respectively, as shown in Fig. 5c. The films remained permanently folded, indicating a homogenous superhydrophobic surface maintaining asymmetric nature that is required to keep the gradient across the thickness intact.

The HP-3 films had undergone complete actuation in 20 sec; however, they unfolded partially over time to attain a final curvature of 0.1 cm^{-1}, as shown in Fig. 5c. Initial curvature might be due to the concentration gradient between the top and bottom surface which saturates quickly, leading to unfolding. The chitosan films with a ratio of hydrophilic SiNPs, i.e., HP-4 and HP-5, do not fold as no gradient was formed.

3.4. pH-responsive behavior of asymmetric films

Owing to the presence of cationic NH^{3+} groups, chitosan is an acid-responsive polymer. Chitosan has been used with other basic responsive polymers, such as carboxymethyl cellulose (CMC) [14] and alginate [15], to show pH-responsive bidirectional actuation. There is no literature available on bidirectional actuation with a single material system. In our work, the obtained asymmetric chitosan film undergoes bidirectional actuation without using any anionic polymer.

The pH-responsive behavior was tested on films CH-Th1, CH-Th2, CH-Th3, and CH-Th4 prepared with a different volume of chitosan solution containing MTS-modified SiNP (1:1) poured over different volumes of chitosan solution keeping the final volume (40 ml) constant as shown in Fig. 2d. pH solutions of pH 1 and pH 4 were prepared by

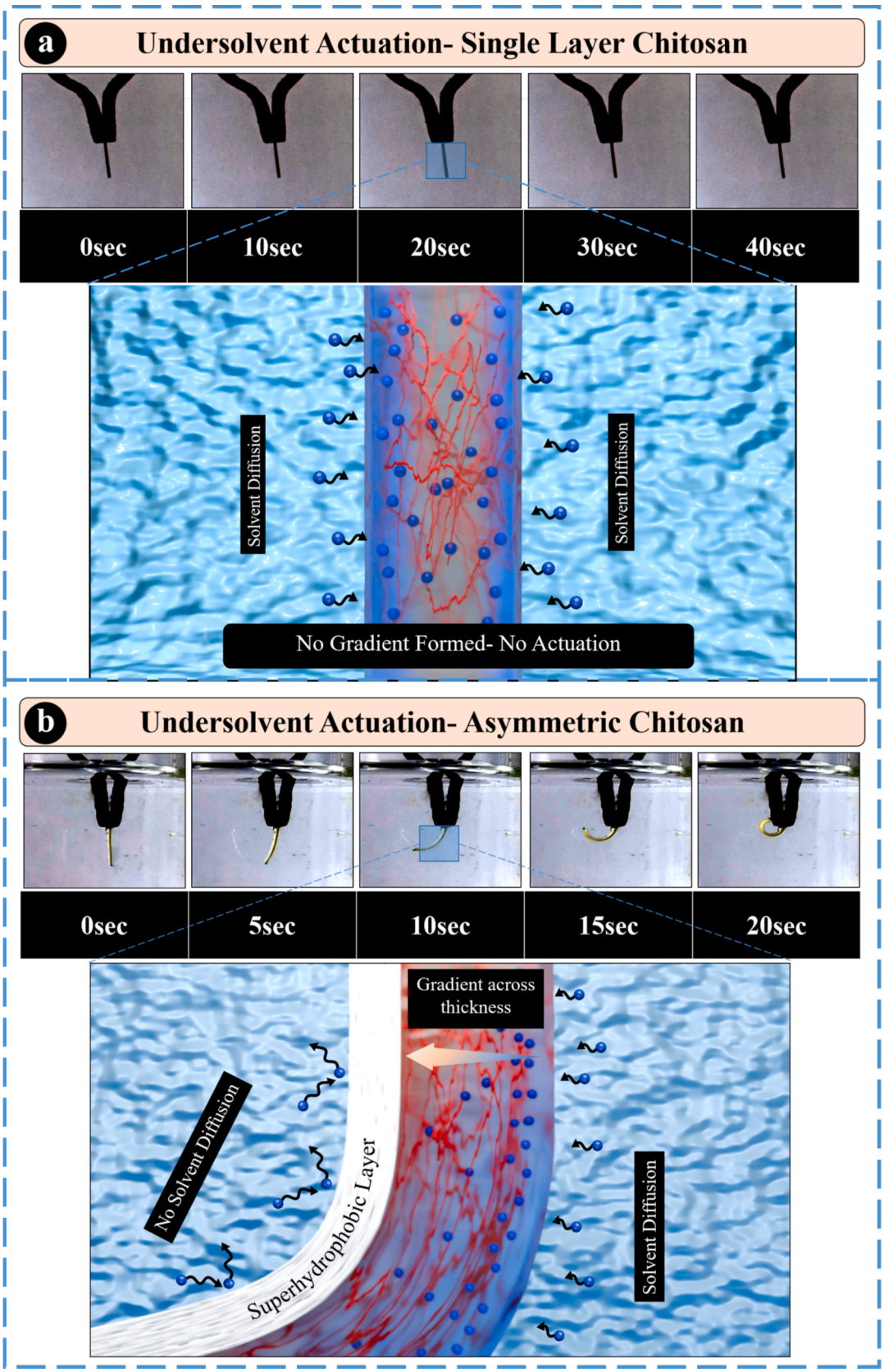

Fig. 3. Schematic representing (a) no actuation of chitosan films when placed inside the solvent due to absence of concentration gradient, (b) actuation mechanism of asymmetric chitosan films (modified with superhydrophobic SiO_2 nanoparticles) when dipped inside the solvent due to formation of the solvent concentration gradient across the thickness of the film.

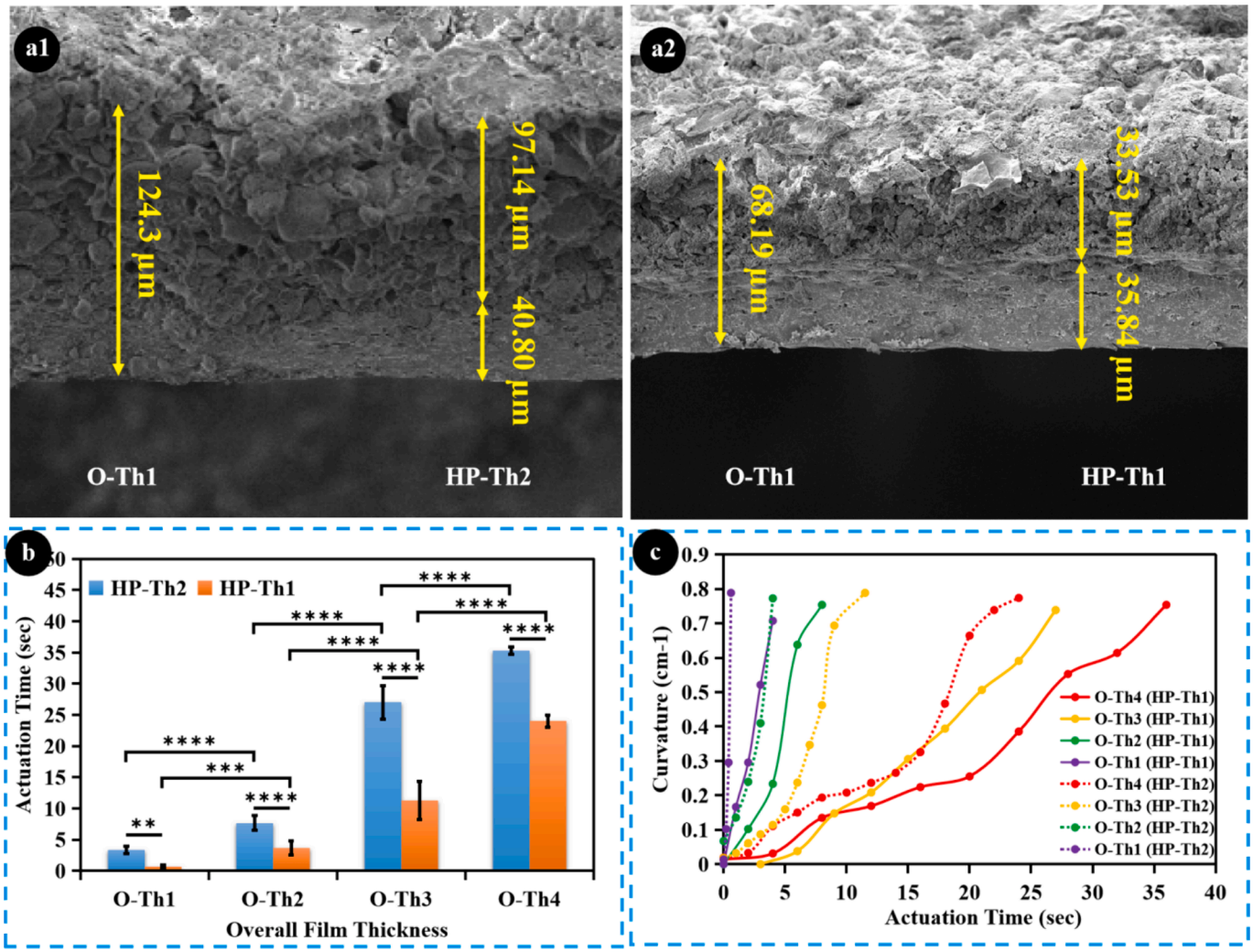

Fig. 4. (a1-a2) SEM images of asymmetric MTS-modified SiNPs/chitosan films indicating an increase in superhydrophobic layer thickness with the increase in the concentration of SiNPs (HP-Th1 and HP-Th2), (b) Plot indicates the actuation time of prepared film with a different superhydrophobic layer thickness (HP-Th1 and HP-Th2) (**$P = 0.0017$, ***$P = 0.0005$, ****$P < 0.0001$, two-way ANOVA) and different overall film thickness (O-Th1, O-Th2, O-Th3 and O-Th4) (****$P < 0.0001$, two-way ANOVA). The effect of layer thickness on actuation time is calculated, and (c) a plot is used to indicate the curvature attained during actuation at an instant of time by asymmetric chitosan films.

diluting 0.1 M HCl, and pH solutions of pH 10 and pH 13 were prepared by diluting 0.1 M NaOH solution. DI water is taken for a neutral pH solution.

Different volumes of chitosan solution without superhydrophobic SiNPs were poured to attain asymmetric films with thicker bottom chitosan layer thickness compared to the top superhydrophobic layer as obtained through SEM images presented in Fig. S3. All the films with different volumes actuated quickly in acidic pH compared to neutral or slightly alkaline pH. Out of all the films prepared with the above technique, the CH-Th4 films resulted in complete anticlockwise actuation in pH 13, as shown in Fig. 6b (Video 1). The mechanism for bidirectional actuation of prepared CH-Th4 films was demonstrated in Fig. 6a. It was observed that the film dipped in an acidic medium actuated in a clockwise direction (towards the superhydrophobic SiNPs side), and in the basic medium, the films actuated in an anticlockwise direction (towards the hydrophilic chitosan side). The CH-Th4 film in pH 1 folds in 12 ± 0.5 sec, whereas folding takes 18 ± 1 sec in pH 4 solution. In an acidic medium, the amine (NH_2) groups in the chitosan chain get protonated to NH_3^+ due to the high concentration of H^+ ions in 0.1 M HCl. Due to the protonation of NH_3^+, the chains repel each other, thus increasing the diffusion rate of the solvent. Faster actuation in a clockwise direction at pH 1 is attributed to the presence of more NH_3^+ groups in pH 1 solution compared to pH 4 (Fig. 6c). In an acidic medium, both the intermolecular chain repulsion and diffusion of the solvent act in the same direction collectively to generate net moment in a clockwise direction. In a basic medium, i.e., pH 13, the anticlockwise actuation takes 200 ± 10 sec. The anticlockwise actuation is due to the high concentration of OH^- ions, which neutralizes the existing protonated NH_3^+ groups present during the preparation of chitosan (1 % acetic acid). The neutralization causes the chain to come closer, thus reducing the diffusion of solvent, leading to shrinkage of the uncrosslinked chitosan side. In pH 13, the two factors, the intermolecular chain leading to shrinkage and diffusion of solvent, act in opposite directions. pH 13 being highly basic leads to the intermolecular chain coming closer, a dominating factor over solvent diffusion, resulting in the net moment of actuation in an anticlockwise direction. At pH 10, the CH-Th4 film folds in 48 ± 3 sec in a clockwise direction as the moment created by the diffusion of the solvent medium dominated the moment generated by the shrinkage of the chitosan film. At pH 7, the film folds completely in a clockwise direction at 21 ± 2 sec due to the diffusion of water into the chitosan matrix. It remains permanently folded as the concentration gradient of water across the film thickness is maintained. For the swelling ratio plot, as shown in Fig. S4, the stability of films after 4 h in acid, base and DI water was confirmed.

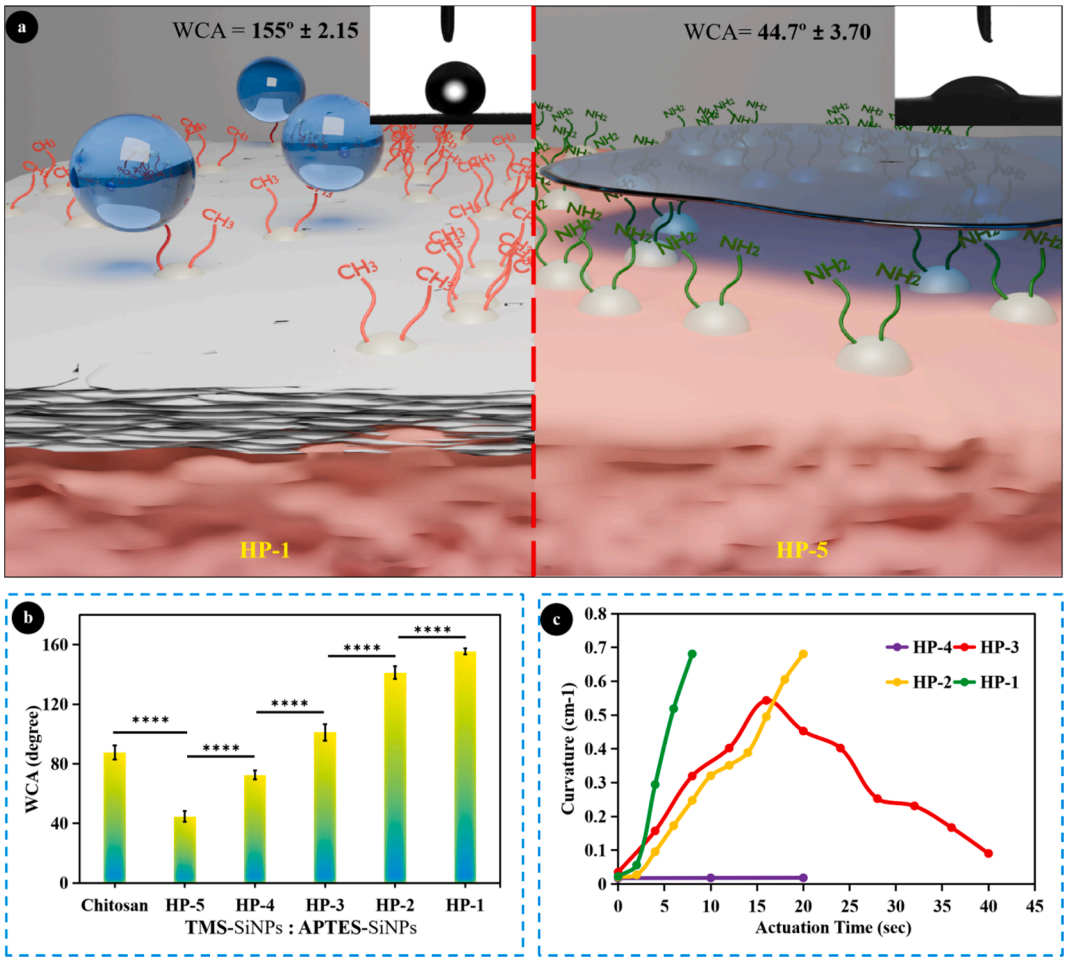

Fig. 5. (a) Schematics representation of asymmetric chitosan films with varied hydrophilicity, $–CH_3$ indicates superhydrophobic surface, $–NH_2$ indicates hydrophilic surface, (b) Plot indicating the water contact angle obtained for prepared asymmetric chitosan films with different hydrophilicity (****$P<0.0001$, one-way ANOVA) and (c) Curvature attained at an instance during actuation of HP-1, HP-2, HP-3 and HP-4 (WCA: HP-1 > HP-2 > HP-3 > HP-4 > HP-5) (Note:- HP-5 is not shown because it doesn't show actuation).

3.5. Superhydrophobic stability of films

The stability of superhydrophobic surfaces is vital for their usage in various biomedical applications. MTS-modified SiNPs (superhydrophobic) consist of $–CH_3$ and –OH (in abundance) groups. When the superhydrophobic SiNPs are mixed in a chitosan solution, they form hydrogen bonding with –OH and $–NH_2$ groups of chitosan chains, creating a stable interface. The superhydrophobic SiNPs, after self-assembly on the surface, bond to neighbouring nanoparticles via hydrogen bonding, forming a thick layer. The asymmetric nature of the prepared films was confirmed by FTIR plots, as shown in Fig. S5. The combined interaction of silica NPs with chitosan and silica-silica interaction leads to a stable asymmetric film, as shown in Fig. 7a.

The chemical stability was investigated by immersing the MTS-modified SiNPs/chitosan films (CH-Th4) in alkaline (0.1 M NaOH), acidic (0.1 M HCl), and salt (1 M NaCl) solution for 10 h, the water contact angle observed were 123.8° ± 3.2, 145.2° ± 4.6, 141.1° ± 2.4 respectively after 10 h as shown in Fig. 7b, 7c and 7d respectively. The samples were stable in acidic and NaCl salt solutions, whereas in the alkaline solution, the water contact angle was reduced from 145.5° ± 4.23 to 123.8° ± 3.2. In 0.1 M NaOH (alkaline) solution, the film actuates in an anticlockwise direction due to shrinkage of chitosan that might disrupt superhydrophobic SiNPs distribution on the surface, causing the decrease of contact angle. The chemical stability was tested in absolute ethanol for 10 h; the obtained contact angle was 146.2° ± 4.2, as shown in Fig. 7e. Ethanol is required for the reversibility of the actuated films.

The superhydrophobic surfaces were subjected to 30 min of UV irradiation to check their stability under harsh conditions. The contact angle obtained after 30 min exposure to UV light was 137.9° ± 3.5, as shown in Fig. 7f. The mechanical stability test was conducted with 400-grit sandpaper with 100 g weight for 50 abrasion cycles (10 cm up and down movement). The contact angle obtained was 141.4° ± 4.3, indicating the high mechanical stability of the superhydrophobic surface, as shown in Fig. 7g.

3.6. In-vitro bacterial assays for actuation-based biomedical applications

Persistent accumulation and proliferation of bacteria and other biomolecules pose significant hurdles in biomedical devices. Bacterial biofouling has been a major concern in medical devices like implants, stents, catheters, and other prostheses. Superhydrophobic surfaces have played a significant role in various mentioned problems. The developed asymmetric chitosan films (Ch-Th4) were tested for bacteria adhesion, bacterial cell viability, and proliferation.

The bacterial adhesion properties of superhydrophobic films and pristine chitosan films were characterized by SEM images. As shown in Fig. 8a, when the *E. coli* and *S. aureus* cells were incubated with the films for 1 h, no bacterium was observed on the MTS-modified superhydrophobic surface, whereas the control, i.e., pristine chitosan had large quantities of bacterial cells adhered. The results indicate the efficiency of MTS-modified superhydrophobic film in inhibiting bacterial

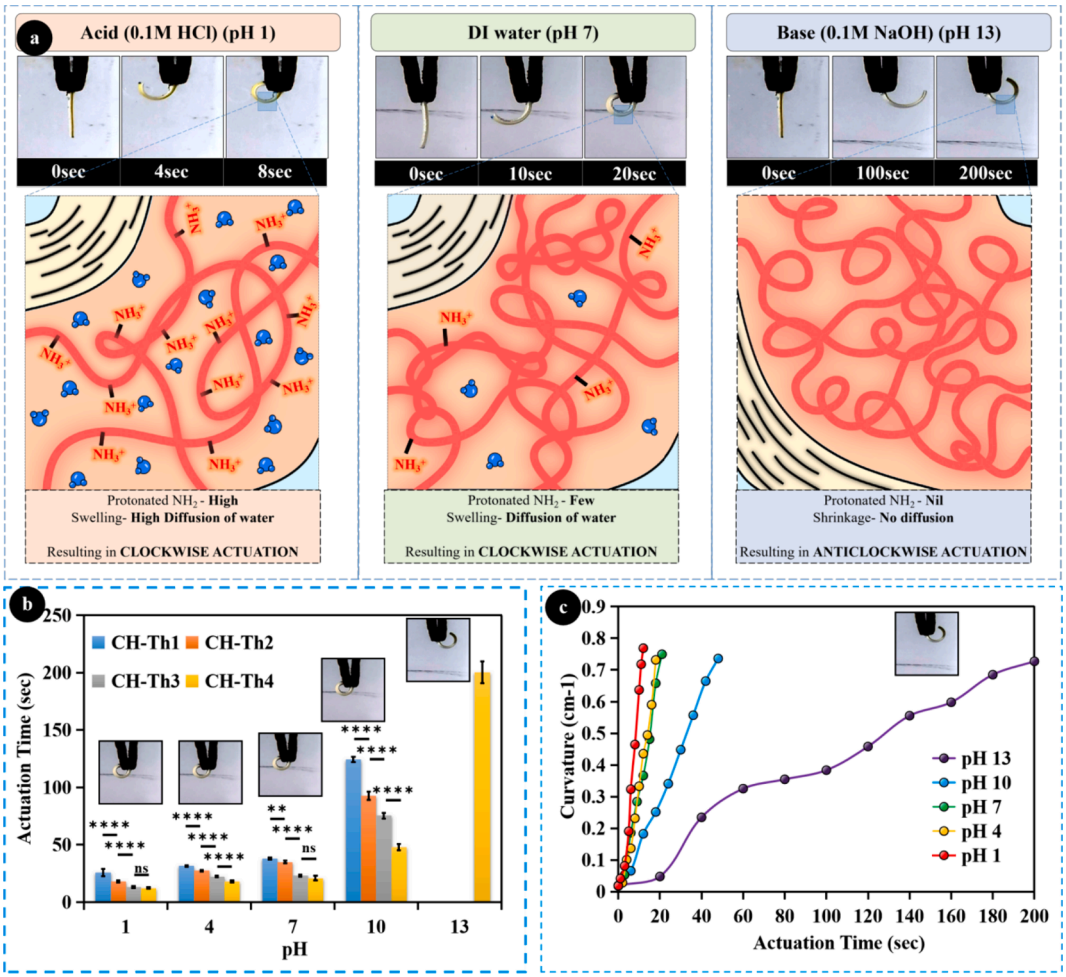

Fig. 6. (a) The pH-responsive mechanism of bidirectional actuation of the prepared CH-Th4 film in the acidic and alkaline solution. (b) plot indicating actuation of prepared films (CH-Th1, CH-Th2, CH-Th3, CH-Th4) at different pH (ns, no statistical significance, $^{**}P = 0.0016$, $^{****}P < 0.0001$, two-way ANOVA), (c) plot indicating the curvature attained while actuating at different pH, at a particular instance of time.

cell adhesion.

For the antibacterial activity of MTS-modified superhydrophobic films, the *E. coli* and *S. aureus* cells were allowed to adhere to the surface for 2 h, and then samples were reversed and slid on agar plates. Pristine chitosan was used as a control. The growth was observed after 24 h of incubation; the control film plates had bacterial colonies, whereas no growth was seen in plates with cells detached from the superhydrophobic surface, indicating the efficient antibacterial activity of MTS-modified superhydrophobic films as shown in Fig. 8b.

The control and MTS-modified superhydrophobic films were UV sterilized for the bacterial infiltration test and kept on the agar surface with the superhydrophobic side face up. The spherical droplet was formed when 50 μl of bacterial cell culture was poured on the superhydrophobic surface. After 24 h of incubation, the plates had no growth on plates with MTS-modified hydrophobic films, and spherical droplets were also maintained, whereas the control plates had visible bacterial growth. Even after 5 days, no growth was seen on the agar plates, indicating excellent bacterial infiltration resistance, as shown in Fig. 8c. Quantitative measurement of antibacterial efficiency by determining OD_{600} absorbance and colony counts upon serial dilution showed excellent anti-fouling properties (Fig. S8).

The obtained superhydrophobic surface of asymmetric films showed excellent antifouling properties and a durable bacteria barrier for 5 days compared to control films. The developed asymmetric films have strong potential for medical tools and devices such as catheters and other implants to prevent bacterial contamination.

3.7. 4D printed asymmetric structure for biomedical applications

Biomedical applications such as stents, catheters, and tools for minimally invasive surgery require complex architectures. Some of the designed closed structures are difficult to modify to attain additional properties such as antifouling, drug delivery, etc. To create complex shapes and structures of soft polymers, a 3D printing strategy is necessary. With the advantage of the self-assembled strategy to attain a superhydrophobic surface, actuating structures can be designed with inherent antifouling properties. To achieve an asymmetric 3D printed structure, the Direct Ink Writing (DIW) printing method was used in this work. The concentration of chitosan and MTS-modified SiNPs was changed to make a printable ink. The modified ink with superhydrophobic silica nanoparticles was printed as another layer to make asymmetric hinges on the printed chitosan structures. Using this method, we could attain an asymmetric layer in situ without switching to other complex procedures to get the superhydrophobic surface.

Planar structures were printed with hinges at specific sites to attain 3d structure. The structures were printed with varying lengths of superhydrophobic layer. The printed structure with a complete bilayer of 35 mm × 5 mm, as shown in Fig. 9a1 (Video 2), resulted in rolling actuation when dipped inside the solution. The structure with a superhydrophobic layer length of 10 mm over a hydrophilic layer of 35 mm length resulted in cross-leg actuation, as shown in Fig. 9a2 (Video 3). The curvature attained was less, with a reduced length of the active part compared to the complete bilayer. The active hinges of the

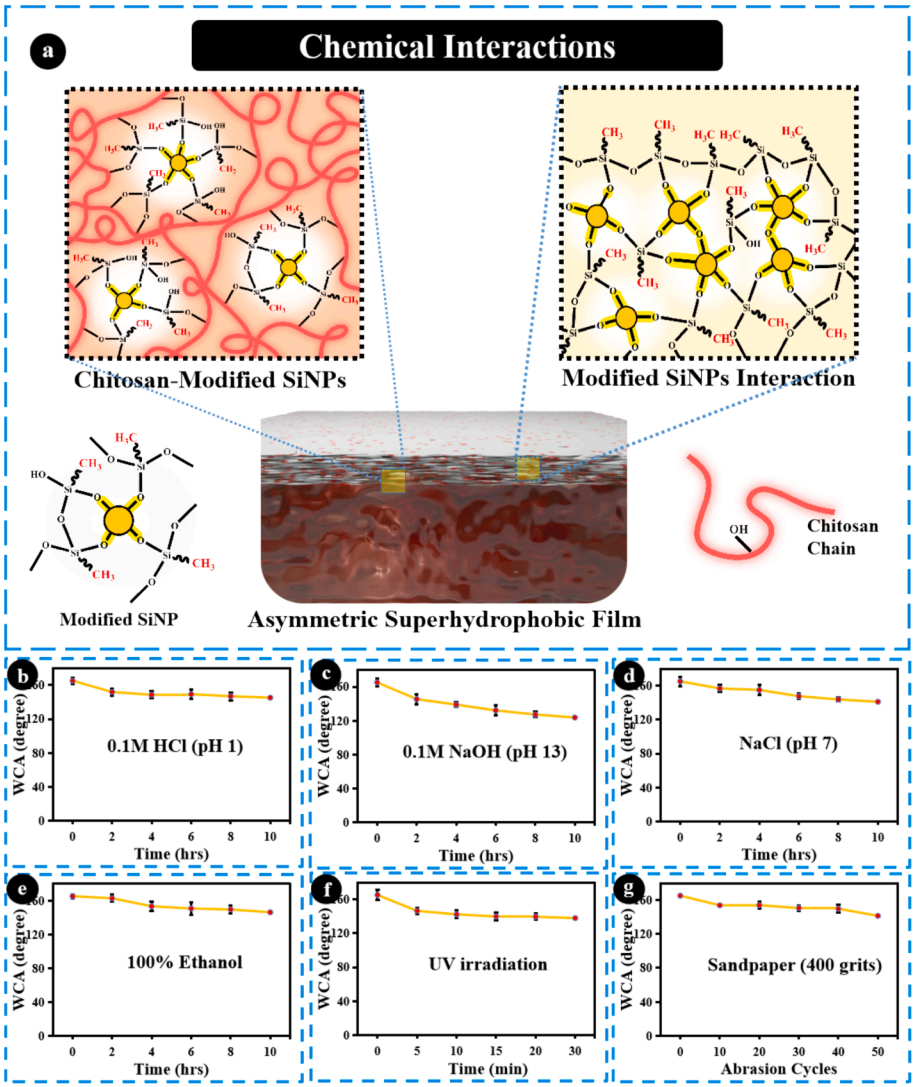

Fig. 7. (a) Mechanism of interface stability between chitosan and MTS-modified SiNPs, Strong interface due to nanoparticles interaction with chitosan chains and interparticle interaction, (b) Plot indicating WCA in 0.1 M HCl after 10 h, (c) Plot indicating WCA in 0.1 M NaOH after 10 h, (d) Plot indicating WCA in 1 M NaCl after 10 h, (e) Plot indicating WCA in absolute ethanol after 10 h, (f) Plot indicating WCA UV irradiation for 30 min, (g) Plot indicating WCA after 50 cycles of sandpaper abrasion.

superhydrophobic layer were reduced to 5 mm on a total structure length of 35 mm. The curvature attained decreases further, giving a U-shaped actuation, as shown in Fig. 9a3 (Video 4). For the final planar structure, the hinges of 5 mm length were made at both sides of the 55 mm length structure in an alternating manner to obtain a W-shaped structure, as shown in Fig. 9a4 (Video 5). The actuated 3D patterns indicate that the hinge length (active part) can be tuned easily to attain a desired structure. The aspect ratio of the base layer also plays a role in determining an output structure. These structures can be used as soft grippers, soft manipulators, and in biomimetic applications.

Furthermore, 3D structures were printed along with planar structures to attain the desired complex 3D structures. The rheological characterisation of the chitosan ink prepared is presented in Fig. S6. Printing a 3D structure of a hydrogel-based system is quite a challenging task. In this work, to obtain tubular structures of different patterns, printing around circular mandrels was done. First, the spiral shape was printed on the mandrel of 5 cm in length, with the silica coating (white layer) on the outside of the initial structure, as shown in Fig. 9b1 (Video 6). After actuation, it was observed that the spiral reversed (inside out) within 2 min with silica coating towards the inner side of the final structure. Open tubular structures with silica coating(outside) were actuated inside the solvent to obtain a tubular structure with silica coating inside, as shown in Fig. 9b2 (Video 7). These reversible, collapsable structures can be helpful in navigating confined spaces and performing functions like drug delivery through actuation.

The requirement of control over actuation to attain desirable shape along with superhydrophobic surface has a significant role in biomedical applications. This morphing characteristic with a superhydrophobic surface can be projected to its usage as a cardiovascular stent, as shown in Fig. 9c. Currently, used drug-eluting stents or bioresorbable stents need to be modified with other polymeric coating and nanoparticles to attain desirable shape changing as well as it performing functions such as drug delivery with antithrombic and antiplatelet surface. In this section, we have demonstrated the ease of developing a complex 3D structure via 3D printing to actuate in the desired shape. The shape morphing can provide a necessary expandable printed structure to open the blocked artery/vein, and the superhydrophobic layer can serve as an anti-platelet adhesive surface.

4. Conclusions

The development of superhydrophobic surfaces holds great promise

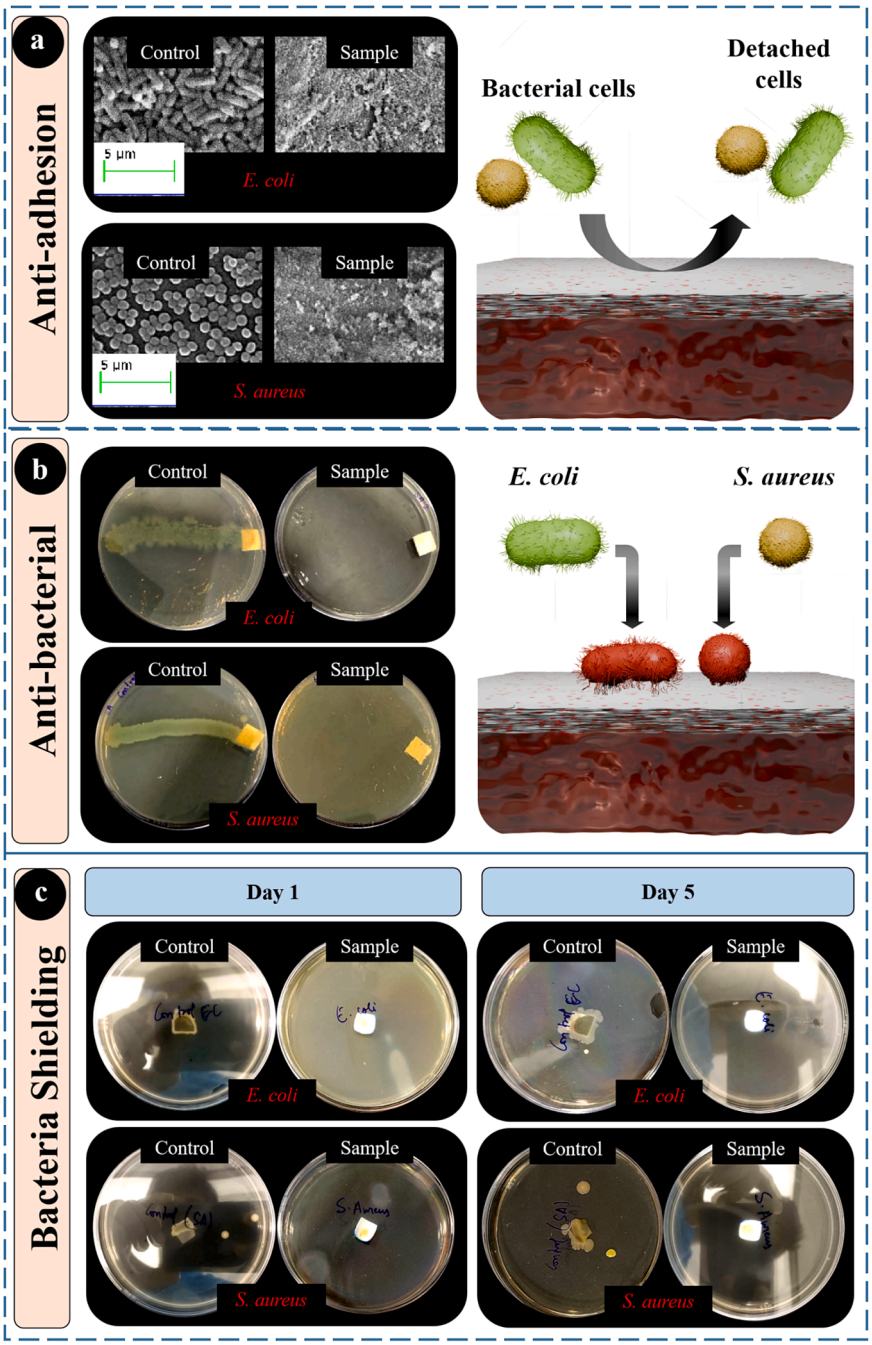

Fig. 8. Pictures showing in-vitro bacterial barrier properties of the superhydrophobic surface against *E. coli* and *S. aureus*. (a) Anti-adhesion, SEM images indicate no adhesion on superhydrophobic samples after 1 h adhesion (b) Anti-bacterial film were streaked on the plate after 1 h growth, no cells growth found after 1 day, (c) Bacterial shielding performance after 5 days indicating the ability of surface not allow bacteria infiltration. Control: Pristine chitosan condition; Sample: MTS-modified superhydrophobic film condition.

in various biomedical applications, offering non-fouling properties required for cell scaffolds, medical devices, and bacterial inhibition. Our study presents a new approach to developing asymmetric chitosan films with superhydrophobic and hydrophilic properties through the self-assembly of MTS-modified silica nanoparticles. The developed film matrix can be tuned to attain the desired bidirectional actuation in different pH solvents. The film exhibits excellent chemical stability to strongly acidic (0.1 M HCl), a strong base (0.1 M NaOH), salt (1 M NaCl) solution, and absolute ethanol and with enhanced mechanical stability to sandpaper abrasion and UV irradiation. The asymmetric film showed superior anti-fouling and anti-bacterial properties to *E. coli* and *S. aureus* cells. Moreover, these asymmetric structures are amenable to 3D printing in situ. Thus, our findings have important implications for designing and developing structures for medical devices.

CRediT authorship contribution statement

Amit Kumar: Writing – review & editing, Writing – original draft, Validation, Methodology, Investigation, Data curation, Conceptualization. **Smruti Parimita:** Writing – review & editing, Writing – original draft, Validation, Data curation. **Kumari Kiran:** Investigation, Data curation. **Nitish R. Mahapatra:** Writing – review & editing, Supervision. **Pijush Ghosh:** Writing – review & editing, Supervision, Resources, Conceptualization.

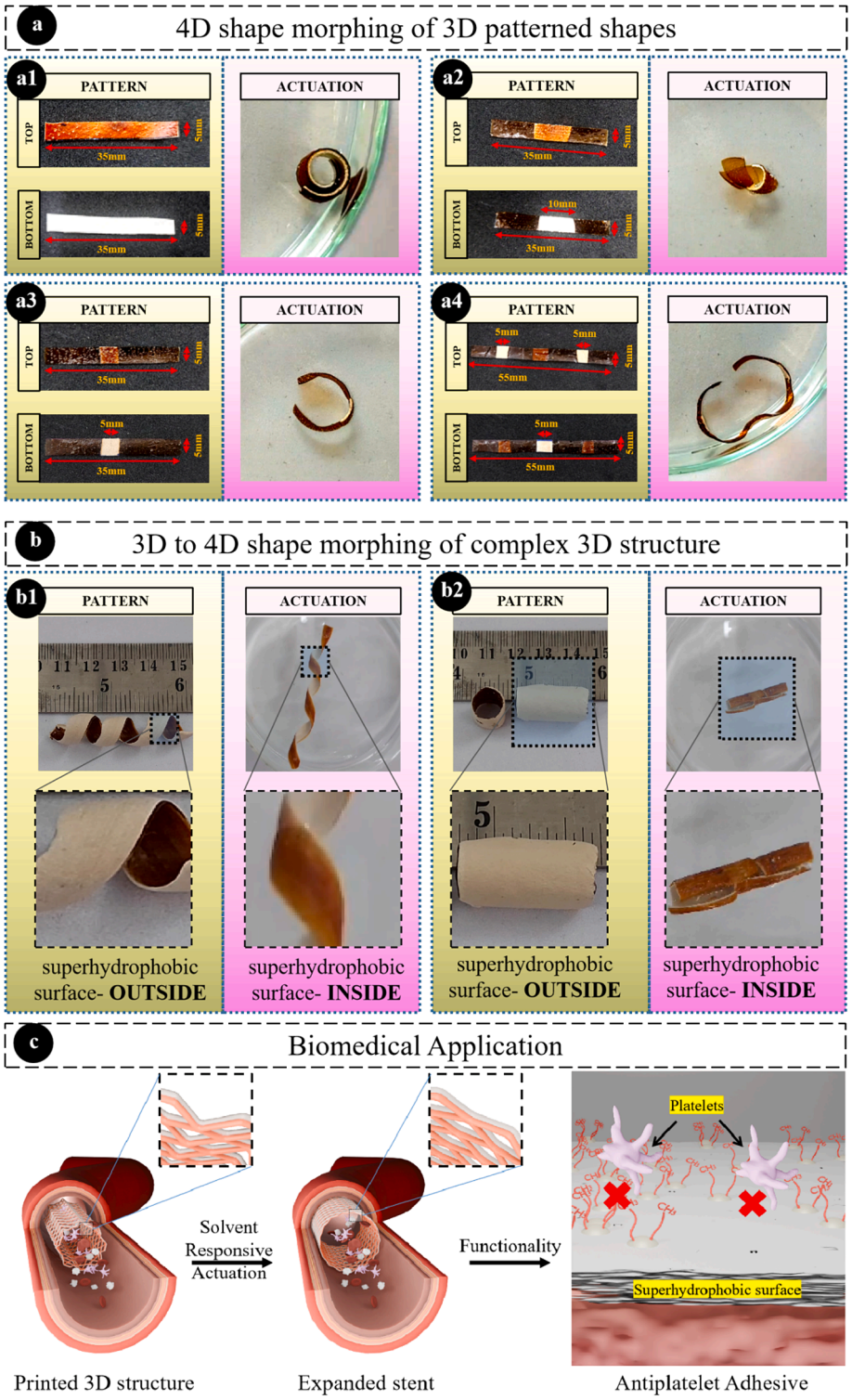

Fig. 9. Actuation pattern of (a) 3D patterned structure, (a1) Rolling actuation for complete bilayer, (a2) Crossleg actuation for large active hinge, (a3) U-shaped actuation for small active hinge, and (a4) W-shaped actuation for alternative superhydrophobic hinges, (b) complex 3D structure, (b1) reversible spiral actuation, (b2) reversible open cylinder, (c) Biomedical application as cardiovascular stent where actuation can provide stent expansion and superhydrophobic surface can provide anti-platelet adhesive surface required to prevent further blockage.

Declaration of competing interest

The authors declare the following financial interests/personal relationships which may be considered as potential competing interests: Pijush Ghosh reports financial support (Project No. CRG/2022/007942) was provided by Science and Engineering Research Board (SERB), Government of India. If there are other authors, they declare that they have no known competing financial interests or personal relationships that could have appeared to influence the work reported in this paper.

Data availability

Data will be made available on request.

Appendix A. Supplementary data

Supplementary data to this article can be found online at https://doi.org/10.1016/j.cej.2024.154772.

References

[1] R.C. Feneley, I.B. Hopley, P.N. Wells, Urinary catheters: history, current status, adverse events and research agenda, J. Med. Eng. Technol. 39 (8) (2015) 459–470, https://doi.org/10.3109/03091902.2015.1085600.

[2] A. Scafa Udriște, A.G. Niculescu, A.M. Grumezescu, E. Bădilă, Cardiovascular stents: a review of past, current, and emerging devices, Materials 14(10) (2021) 2498, https://doi.org/10.3390%2Fma14102498.

[3] O.M. Omisore, S. Han, J. Xiong, H. Li, Z. Li, L. Wang, A review on flexible robotic systems for minimally invasive surgery, IEEE Trans. Syst., Man, Cybernet.: Syst. 52 (1) (2020) 631–644, https://doi.org/10.1109/TSMC.2020.3026174.

[4] S. Adepu, S. Ramakrishna, Controlled drug delivery systems: current status and future directions, Molecules 26 (19) (2021) 5905, https://doi.org/10.3390%2Fmolecules26195905.

[5] V. Levering, C. Cao, P. Shivapooja, H. Levinson, X. Zhao, G.P. López, Urinary catheter capable of repeated on-demand removal of infectious biofilms via active deformation, Biomaterials 77 (2016) 77–86, https://doi.org/10.1016/j.biomaterials.2015.10.070.

[6] E. Gultepe, J.S. Randhawa, S. Kadam, S. Yamanaka, F.M. Selaru, E.J. Shin, A. N. Kalloo, D.H. Gracias, Biopsy with thermally-responsive untethered microtools, Adv. Mater. (Deerfield Beach, Fla.) 25 (4) (2013), https://doi.org/10.1002/adma.201203348.

[7] G. Decroly, B. Mertens, P. Lambert, A. Delchambre, Design, characterization and optimization of a soft fluidic actuator for minimally invasive surgery, Int. J. Comput. Assist. Radiol. Surg. 15 (2020) 333–340, https://doi.org/10.1007/s11548-019-02081-2.

[8] B. Liu, H. Li, F. Meng, Z. Xu, L. Hao, Y. Yao, H. Zhu, C. Wang, J. Wu, S. Bian, W. W. Lu, 4D printed hydrogel scaffold with swelling-stiffening properties and programmable deformation for minimally invasive implantation, Nat. Commun. 15 (1) (2024) 1587, https://doi.org/10.1038/s41467-024-45938-0.

[9] J. Li, Q. Ma, Y. Xu, M. Yang, Q. Wu, F. Wang, P. Sun, Highly bidirectional bendable actuator engineered by LCST–UCST bilayer hydrogel with enhanced interface, ACS Appl. Mater. Interfaces 12 (49) (2020) 55290–55298, https://doi.org/10.1021/acsami.0c17085.

[10] D. Podstawczyk, M. Nizioł, P. Szymczyk-Ziółkowska, M. Fiedot-Toboła, Development of thermoinks for 4D direct printing of temperature-induced self-rolling hydrogel actuators, Adv. Funct. Mater. 31 (15) (2021) 2009664, https://doi.org/10.1002/adfm.202009664.

[11] X. Liu, J. Hu, J. Yang, L. Peng, J. Tang, X. Wang, R. Huang, J. Liu, K. Liu, T. Wang, X. Liu, Fully reversible and super-fast photo-induced morphological transformation of nanofilms for high-performance UV detection and light-driven actuators, Adv. Sci. (2024) 2307165, https://doi.org/10.1002/advs.202307165.

[12] A. Saifi, C. Negi, K. Kumar, Visible light responsive soft actuator based on functional anthracene dye, Eur. Polym. J. 171 (2022) 111176, https://doi.org/10.1016/j.eurpolymj.2022.111176.

[13] A. Saifi, C. Negi, A.P. Singh, K. Kumar, Visible light responsive soft actuator based on PVA-DR1, ChemistrySelect 8 (39) (2023) e202301628, https://doi.org/10.1002/slct.202301628.

[14] X. Zhao, J. Jiang, Z. Liu, Z. Liu, G. Li, Thermal and near-infrared light-responsive hydrogel actuators with spatiotemporally developed polypyrrole patterns, ACS Appl. Mater. Interfaces 16 (7) (2024) 9286–9292, https://doi.org/10.1021/acsami.3c17885.

[15] H.E. Fowler, P. Rothemund, C. Keplinger, T.J. White, Liquid crystal elastomers with enhanced directional actuation to electric fields, Adv. Mater. 33 (43) (2021) 2103806, https://doi.org/10.1002/adma.202103806.

[16] Y. Shin, M.Y. Choi, J. Choi, J.H. Na, S.Y. Kim, Design of an electro-stimulated hydrogel actuator system with fast flexible folding deformation under a low electric field, ACS Appl. Mater. Interfaces 13 (13) (2021) 15633–15646, https://doi.org/10.1021/acsami.1c00883.

[17] J. Wang, X. Zhang, A. Wang, X. Hu, L. Deng, L. Lou, H. Shen, The sythesnis and simulations of solvent-responsive bilayer hydrogel, Polymer 204 (2020) 122801, https://doi.org/10.1016/j.polymer.2020.122801.

[18] S. Parimita, A. Kumar, H. Krishnaswamy, P. Ghosh, Solvent triggered shape morphism of 4D printed hydrogels, J. Manuf. Process. 85 (2023) 875–884, https://doi.org/10.1016/j.jmapro.2022.11.065.

[19] N. Gupta, A. Kumar, P.K. Vaddavalli, N.R. Mahapatra, A. Varshney, P. Ghosh, Efficient reduction of the scrolling of Descemet membrane endothelial keratoplasty grafts by engineering the medium, Acta Biomater. 171 (2023) 239–248, https://doi.org/10.1016/j.actbio.2023.09.024.

[20] A. Rath, S. Mathesan, P. Ghosh, Folding behavior and molecular mechanism of cross-linked biopolymer film in response to water, Soft Matter 12 (45) (2016) 9210–9222, https://doi.org/10.1039/C6SM01994C.

[21] Z. Han, P. Wang, G. Mao, T. Yin, D. Zhong, B. Yiming, X. Hu, Z. Jia, G. Nian, S. Qu, W. Yang, Dual pH-responsive hydrogel actuator for lipophilic drug delivery, ACS Appl. Mater. Interfaces 12 (10) (2020) 12010–12017, https://doi.org/10.1021/acsami.9b21713.

[22] A. Kumar, R. Rajamanickam, J. Hazra, N.R. Mahapatra, P. Ghosh, Engineering the nonmorphing point of actuation for controlled drug release by hydrogel bilayer across the pH spectrum, ACS Appl. Mater. Interfaces 14 (50) (2022) 56321–56330, https://doi.org/10.1021/acsami.2c16658.

[23] M. Gierszewska, J. Ostrowska-Czubenko, E. Chrzanowska, pH-responsive chitosan/alginate polyelectrolyte complex membranes reinforced by tripolyphosphate, Eur. Polym. J. 101 (2018) 282–290, https://doi.org/10.1016/j.eurpolymj.2018.02.031.

[24] Z. Shao, S. Wu, Q. Zhang, H. Xie, T. Xiang, S. Zhou, Salt-responsive polyampholyte-based hydrogel actuators with gradient porous structures, Polym. Chem. 12 (5) (2021) 670–679, https://doi.org/10.1039/D0PY01492C.

[25] R.K. Meena, S.D. Rapaka, R. Pratoori, R.K. Annabattula, P. Ghosh, An embedded interface regulates the underwater actuation of solvent-responsive soft grippers, Soft Matter 18 (2) (2022) 372–381, https://doi.org/10.1039/D1SM01229K.

[26] Y. Shao, J. Zhao, Y. Fan, Z. Wan, L. Lu, Z. Zhang, W. Ming, L. Ren, Shape memory superhydrophobic surface with switchable transition between “Lotus Effect” to “Rose Petal Effect”, Chem. Eng. J. 382 (2020) 122989 https://doi.org/10.1016/j.cej.2019.122989.

[27] R. Jiang, L. Hao, L. Song, L. Tian, Y. Fan, J. Zhao, C. Liu, W. Ming, L. Ren, Lotus-leaf-inspired hierarchical structured surface with non-fouling and mechanical bactericidal performances, Chem. Eng. J. 398 (2020) 125609, https://doi.org/10.1016/j.cej.2020.125609.

[28] L.C. Pan, S.Y. Hsieh, W.C. Chen, F.T. Lin, C.H. Lu, Y.L. Cheng, H.W. Chien, H. Yang, Self-assembly of shark scale-patterned tunable superhydrophobic/antifouling structures with visual color response, ACS Appl. Mater. Interfaces 15 (29) (2023) 35311–35320, https://doi.org/10.1021/acsami.3c03086.

[29] Y. Li, L.Y. Zhang, C. Zhang, Z.R. Zhang, L. Liu, Bioinspired antifouling Fe-based amorphous coating via killing-resisting dual surface modifications, Sci. Rep. 12 (1) (2022) 819, https://doi.org/10.1038/s41598-021-04746-y.

[30] H.P. Lin, L.J. Chen, Direct observation of wetting behavior of water drops on single micro-scale roughness surfaces of rose petal effect, J. Colloid Interface Sci. 603 (2021) 539–549, https://doi.org/10.1016/j.jcis.2021.06.132.

[31] X. Yang, Y. Chen, X. Zhang, P. Xue, P. Lv, Y. Yang, L. Wang, W. Feng, Bioinspired light-fueled water-walking soft robots based on liquid crystal network actuators with polymerizable miniaturized gold nanorods, Nano Today 43 (2022) 101419, https://doi.org/10.1016/j.nantod.2022.101419.

[32] Z. Wang, J. Xiong, Y. Liao, M. Xie, D. Yang, C. Zhang, Y. Chen, Z. Zou, Bionic Janus membranes to manipulate bubbles underwater for hydrogen evolution reactions, Chem. Eng. J. 474 (2023) 145352, https://doi.org/10.1016/j.cej.2023.145352.

[33] X. Yan, B. Ji, L. Feng, X. Wang, D. Yang, K.F. Rabbi, Q. Peng, M.J. Hoque, P. Jin, E. Bello, S. Sett, Particulate–droplet coalescence and self-transport on superhydrophobic surfaces, ACS Nano 16 (8) (2022) 12910–12921, https://doi.org/10.1021/acsnano.2c05267.

[34] S. Li, P. Xiao, W. Zhou, Y. Liang, S.W. Kuo, T. Chen, Bioinspired nanostructured superwetting thin-films in a self-supported form enabled “miniature umbrella” for weather monitoring and water rescue, Nano-Micro Lett. 14 (2022) 1–16, https://doi.org/10.1007/s40820-021-00775-4.

[35] Y. Yang, H. Shen, J. Qiu, Fabrication of biomimetic robust self-cleaning superhydrophobic wood with canna-leaf-like micro/nanostructure through morph-genetic method improved water-, UV-, and corrosion resistance properties, J. Mol. Struct. 1219 (2020) 128616, https://doi.org/10.1016/j.molstruc.2020.128616.

[36] M.A. Azeem, D.U. Lawal, H. Al Abdulgader, T.N. Baroud, Enhanced performance of superhydrophobic polyvinylidene fluoride membrane with sandpaper texture for highly saline water desalination in air-gap membrane distillation, Desalination 528 (2022) 115603, https://doi.org/10.1016/j.desal.2022.115603.

[37] N. Atthi, M. Dielen, W. Sripumkhai, P. Pattamang, R. Meananeatra, P. Saengdee, O. Thongsook, N. Ranron, K. Pankong, W. Uahchinkul, J. Supadech, Fabrication of high aspect ratio micro-structures with superhydrophobic and oleophobic properties by using large-area roll-to-plate nanoimprint lithography, Nanomaterials 11 (2) (2021) 339, https://doi.org/10.3390/nano11020339.

[38] W. Huang, X. Tang, Z. Qiu, W. Zhu, Y. Wang, Y.L. Zhu, Z. Xiao, H. Wang, D. Liang, J. Li, Y. Xie, Cellulose-based superhydrophobic surface decorated with functional groups showing distinct wetting abilities to manipulate water harvesting, ACS Appl. Mater. Interfaces 12 (36) (2020) 40968–40978, https://doi.org/10.1021/acsami.0c12504.

[39] F. Sahin, N. Celik, A. Ceylan, S. Pekdemir, M. Ruzi, M.S. Onses, Antifouling superhydrophobic surfaces with bactericidal and SERS activity, Chem. Eng. J. 431 (2022) 133445, https://doi.org/10.1016/j.cej.2021.133445.

[40] T. Iline-Vul, S. Bretler, S. Cohen, I. Perelshtein, N. Perkas, A. Gedanken, S. Margel, Engineering of superhydrophobic silica microparticles and thin coatings on polymeric films by ultrasound irradiation, Mater. Today Chem. 21 (2021) 100520, https://doi.org/10.1016/j.mtchem.2021.100520.